Atmospheric Research 267 (2022) 105973

Contents lists available at ScienceDirect

Atmospheric Research

journal homepage: www.elsevier.com/locate/atmosres

Lightning forecasting in Bangladesh based on the lightning potential index and the electric potential

Khan Md Golam Rabbani [a], Md Jafrul Islam [b], Alexandre O. Fierro [c,d,e], Edward R. Mansell [d], Pappu Paul [a,*]

[a] Department of Meteorology, University of Dhaka, Dhaka 1000, Bangladesh
[b] Department of Physics, University of Dhaka, Dhaka 1000, Bangladesh
[c] Cooperative Institute for Mesoscale Meteorological Studies, Norman, OK, United States
[d] NOAA/National Severe Storms Laboratory, Norman, OK, United States
[e] Zentralanstalt für Meteorologie und Geodynamik, Department of Forecasting Models – ZAMG, Vienna, Austria

ARTICLE INFO

Keywords:
Lightning Prediction
WRF-ELEC
LPI
NASA LIS
Satellite
Cloud Electrification

ABSTRACT

This work documents the performances of diagnostic and explicit lightning forecasts for selected high impact weather events over Bangladesh. The lightning flashes are calculated by three methods: (1) a diagnostic lightning parameterization that bases its algorithm on the level of neutral buoyancy from a convective parameterization scheme, (2) lightning potential index (LPI) using local graupel and ice contents, and (3) explicit prediction of electric fields and lightning initiation from WRF-ELEC. Five lightning events that occurred on 02 April 2019, 17 May 2019, 20 April 2020, 26 May 2020, and 20 May 2021 were examined to evaluate the forecasting capability of each scheme for the lightning over a 24-h forecast period. Prior to diagnosing lightning activity, the composite radar reflectivity and the neighborhood score metrics (ETS, FSS) for hourly rainfall were analyzed to determine if the simulated precipitation structure is consistent with the observations. Analyses based on performance diagrams were also included for a better illustration of how simulations perform on predicting precipitation. The spatial distribution of LPI and lightning flashes is compared against the NASA Lightning Imaging Sensor (LIS) dataset. The qualitative results show that in most of the studied cases, there is a good agreement between the observations and the WRF-ELEC-based simulations in terms of detecting the primary regions of lightning activity. The LPI based predictions perform also considerably well. The results from this endeavor constitute an essential initiative towards the implementation of an effective operational lightning warning system to mitigate lightning-related hazards in Bangladesh and northeast India.

1. Introduction

Lightning is a hazardous weather phenomenon that occurs frequently with a global average rate of 46 flashes per second (Albrecht et al., 2016; Cecil et al., 2014; Lutgens et al., 2013). Approximately 6000–24,000 people are killed by lightning strikes yearly around the world (Holle, 2008). In Asia, Bangladesh is in a region characterized by relatively high flash densities (Christian et al., 2003; Markowski and Richardson, 2011). As a consequence of lightning-induced deaths, Bangladesh declared lightning strikes a disaster in 2016 (Dewan et al., 2017). Due to the increasing mortality rate and losses of wealth, lightning prediction has become a core topic investigated by scientists (Yair, 2018).

In this regard, several meteorological (thermodynamic and/or kinematic) indices such as the Convective Available Potential Energy (CAPE), Cloud Physics Thunder Parameter (CPTP), Total Totals Index (TTI), K-Index (KI), Lifted Index (LI), Potential Lightning Region (PLR), etc. have been used to forecast the probability of lightning activity (Bright et al., 2005; Zepka et al., 2014). In recent works (i.e., Deierling and Petersen, 2008; Fierro and Reisner, 2011; Lynn et al., 2012; McCaul Jr et al., 2009; Yair et al., 2010), some of the main physical processes related to lightning have been studied from different standpoints such as control laboratory settings, numerical simulations, observational investigations, and theoretical studies. There are two different techniques to forecast lightning: the first is based on the physics of cloud electrification (explicit), and the second is based on clouds microphysics and

* Corresponding author.
E-mail address: pappu.paul@du.ac.bd (P. Paul).

https://doi.org/10.1016/j.atmosres.2021.105973
Received 11 August 2021; Received in revised form 8 December 2021; Accepted 12 December 2021
Available online 16 December 2021

dynamics (diagnostic). As the latter approach does not include additional prognostic equations for electrical variables, it remains by design more computationally affordable for real time use (Gharaylou et al., 2019). In early research efforts, the KI index (George, 1960), which is a measure of the thunderstorm potential based on the temperature lapse rate, moisture content of the lower troposphere, and the vertical extent of the moist layer, was used to forecast lightning by assuming that every thunderstorm produced lightning (Sturtevant, 1995). Williams et al. (1992) showed a positive correlation between Convective Available Potential Energy (CAPE) and lightning. Other parameters, that mainly depend on cloud thermodynamic and dynamic formulations rather than microphysics principles, such as the Lifted Index (Galway, 1956), Total Totals Index (TTI), Convective Inhibition (CIN), etc. were also be used to predict lightning (Ackerman and Knox, 2012; Bright et al., 2005). These diagnostic prediction methods, however, differ from region to region. Hence, more physics-based prediction methods became increasingly more important for forecasting lightning with a higher degree of accuracy and, arguably, realism. Lynn and Yair (2010) and Yair et al. (2010) introduced the Lightning Potential Index (LPI), which is a measure of the charge generation and separation within convective clouds. They showed a positive correlation between rainfall and observed lightning density. Based on this, they suggested that the LPI could be used to forecast the potential for the occurrence of lightning. The LPI computational scheme was later implemented in the Weather Research and Forecasting (WRF) mesoscale model (Skamarock et al., 2019). Dementyeva et al. (2015) tested different microphysics schemes implemented in WRF to evaluate the performance of the LPI in the prediction of lightning events and found that the LPI underestimates the possible regions of thunderstorms. Fiori et al. (2016) found that the LPI was, overall, a good regional predictor of lightning activity.

Ice and graupel are the chief charge carriers in thunderclouds, as detected in clouds (e.g., Gardiner et al., 1985) and studied in laboratory experiments (e.g., Jayaratne et al., 1983; Reynolds et al., 1957; Takahashi, 1978). Miller et al. (2001) suggested that the updraft speed and the graupel number concentration could serve as the two main parameters to predict lightning rate. Observational studies verified that lightning occurrence required the presence of a strong updraft in the mixed phase region characterized by the presence of appreciable amounts of ice crystals, supercooled cloud droplets and graupel pellets (Deierling and Petersen, 2008; Lang et al., 2004; Tessendorf et al., 2005; Williams et al., 1992). Several numerical studies estimated the lightning rates and other related electrical processes by evaluating lightning events and model output (Zepka et al., 2014). Studies such as Takahashi (1984), Mansell et al. (2010), Mansell et al. (2005) Barthe et al. (2010) focused on electrification and lightning parameterization schemes in cloud-resolving models. A more explicit prediction of lightning (i.e., vs diagnostic) based on macroscopic in-cloud electrification processes can be achieved using an extra package (referred to as ELEC) in the WRF model. The explicit electrification code was coupled with the NSSL microphysics scheme in WRF (referred to as WRF-ELEC). Fierro et al. (2013) described its implementation within WRF. The electric potential method (POT at 7 km altitude), introduced by Dementyeva et al. (2015), for predicting where cloud-to-ground lightning may occur can also be calculated using this package, but is not used here. Gharaylou et al. (2019) used WRF-ELEC to calculate the electric potential (POT) and compared it with LPI for predicting lightning activity for four events that occurred in northern Iran. They concluded based on both qualitative and quantitative evaluation that the horizontal patterns of POT and LPI were in good agreement with the locations of lightning occurrence.

Although research on lightning activity has received mounting interest worldwide, only a few studies have focused on Bangladesh. Using the WRF-ARW model, Das et al. (2015) studied the composite characteristics of pre-monsoon (March to May) thunderstorms and conducted several modeling experiments of thunderstorms over northeast India and adjoining Bangladesh by validating model output with satellite, radar and ground-based observations. Some other notable studies (e.g., Ahasan et al., 2015; Karmakar et al., 2017; Karmakar and Alam, 2017; Litta and Mohanty, 2008; Rabbani et al., 2021; Yamane et al., 2013) analyzed the atmospheric instability and the thermodynamic conditions of thunderstorms over northeast India using CAPE, wind shear, and other relevant meteorological parameters. Das et al. (2014) conducted a coordinated field experiment focusing on severe thunderstorm observations and regional modeling (STORM) over the south Asian region and analyzed thunderstorm characteristics, synoptic conditions, thermodynamic features, along with other environmental factors that are known to trigger severe storms over the region. Al-Amin Hoque et al. (2019) investigated lightning casualties in Bangladesh from 2016 to 2018 reporting a fatality rate of 1.76 per million people per year. Umakanth et al. (2020) calculated several stability parameters such as K Index (KI), Lifted Index (LI) and Total Totals Index (TTI), Convective Available Potential Energy (CAPE) and Total Perceptible Water (TPW) associated with lightning flashes over Bangladesh using ERA-Interim dataset. Most of these studies mentioned earlier analyzed meteorological parameters and casualties due to lightning. Choudhury et al. (2020) simulated the lightning flash rates of a thunderstorm case on May 4, 2013 and compared the results with TRMM-LIS observed flashes. Mohan et al. (2021) simulated lightning flash counts over Maharashtra, India using different lightning parameterization schemes available in WRF and validated the simulated flashes for four cases using ground-based observations from the Maharashtra Lightning Detection Network (LDN). Despite these pioneering efforts, there are until present no studies that utilized an explicit cloud electrification model to forecast lightning over Bangladesh. The main goal of this study is to therefore test three lightning prediction methods (LPI, PR92, and explicit lightning) over Bangladesh. LPI and PR92 are diagnosed from the model state whereas explicit lightning depends on predicted electrification physics within the thundercloud. Both types of methods could be very helpful tools for identifying regions of lightning occurrence and for estimating lightning flash counts. This study, therefore, serves as an essential first approach to forecast lightning activity in Bangladesh using a numerical model at the cloud scale.

2. Methodology and data

2.1. Lightning cases

Based primarily on the availability of observed lightning data from the NASA's Lightning Imaging Sensor (LIS), five high impact cases were selected for this evaluation. LIS observations were employed because, currently, these are the only freely accessible lightning data source over Bangladesh. These five cases include events that occurred on 02 April 2019, 17 May 2019, 20 April 2020, 26 May 2020 and 20 May 2021. Precipitation, cloud coverage, instability indices and intensity of thunderstorms associated with lightning were also considered.

2.2. Model driving datasets

The Global Forecast System (GFS) is a forecasting model developed and designed by the National Centers for Environmental Prediction (NCEP). The six-hourly $1^\circ \times 1^\circ$ lat-lon gridded NCEP FNL (NCEP, 2000) operational global analysis datasets were downscaled to derive the initial and boundary conditions for the simulations herein.

2.3. Observational data

INSAT-3D is an advanced meteorological satellite launched in 2013 by India. It consists of an atmospheric sounder and an imager. Earth imageries in six wavelengths are generated by the multispectral imaging system (optical radiometer). The datasets and blended images of thermal infrared and visible channels are collected from the Meteorological and Oceanographic Satellite Data Archival Centre (www.mosdac.gov.in) and used to determine the cloud coverage of each lightning case

over the study regions.

A space-based lightning sensor named Lightning Imaging Sensor (LIS) mounted on the International Space Station (ISS) is used to estimate the variability of and to detect the distribution of total lightning (i.e., intra-cloud plus cloud-to-ground lightning) in the Earth's tropical and mid-latitude regions. The ISS LIS instrument measures the radiant optical energy, records the time of occurrence of lightning events, and detects the location during both day and night with a 24-h average detection efficiency of 70%. LIS data can also be used for lightning-atmosphere interaction studies as well as for severe storm detection and analysis. The final quality-controlled datasets (Blakeslee, 2020) are used in the present study to validate model predicted lightning location and flash counts. These lightning products are publicly available with a temporal range of 1 min to 1 h and a spatial resolution ranging from 4 to 8 km.

The multi-satellite precipitation dataset derived from the Integrated Multi-satellitE Retrievals for GPM (IMERG) of NASA (National Aeronautics and Space Administration) is also used to compute score matrices. This 10-km resolution product is produced at the NASA Goddard Information Services Center and Earth Sciences Data (Huffman et al., 2019). The GPM IMERG combines information from several low-Earth-orbit satellites (GPM satellite constellation) equipped with passive microwave radiometers (Torcasio et al., 2021) for estimating precipitation over the majority of the Earth's surface. The principal satellite of the GPM constellation is the NASA/JAXA (Japan Aerospace Exploration Agency) GPM Core Observatory, which possesses a dual-frequency Ku/Ka-band precipitation radar and the GPM Microwave Imager.

BAF, Bangladesh Air Force (www.mtrwf.com) has two operational C-Band Doppler Weather Radars (DWR) in Chittagong (Lat: 22.25, Lon: 91.8) and Jashore (Lat: 23.18 N, Lon: 89.16 E) districts in Bangladesh. The spatial coverage of these radars is approximately 480 km. From early 2018, these radars mainly provide reflectivity (dBZ) and rainfall (mm) every minute. The simulated reflectivity fields are validated against the reflectivity observed by Jashore (MTR-DWR) for all cases.

2.4. Model description and setup

2.4.1. WRF-ARW model

The WRF-ARW model has four lightning parameterization options. These lightning options can estimate LPI and flash rate, both of which are analyzed in the present study. The lightning parameterizations based on Yair et al. (2010) and on Price and Rind (1992) were evaluated herein.

2.4.1.1. LPI calculation. According to Yair et al. (2010), the LPI is defined as the volume integral of the total mass flux of liquid water and ice in a developing thundercloud within the "charging zone" (0 °C to −20 °C). It usually represents the potential of the thundercloud to separate electrical charge via the non-inductive ice-graupel mechanism, but it does not explicitly calculate the resulting electric field. LPI changes with time since it is estimated from the kinematic and microphysical model fields in every grid point and at each time step. So, in short, the LPI is a measure of the potential for charge generation and separation for lightning initiation. The basic formulation is as follows:

$$LPI = \frac{1}{V}\iiint \varepsilon w^2 dxdydz \tag{1}$$

Where, w is the vertical wind component (m s^{-1}), V is the cloud volume in the charging zone, and ε is a dimensionless number that depends on the mixing ratios of the hydrometeor components with a value ranging from 0 to 1.

$$\varepsilon = 2\frac{(Q_i Q_l)^{0.5}}{Q_i + Q_l} \tag{2}$$

Where, Q_i is the ice fractional mixing ratio (kg kg^{-1}) and Q_l is the total liquid water mass mixing ratio (kg kg^{-1}). Q_i is defined as follows,

$$Q_i = q_g\left[\frac{(q_s q_g)^{0.5}}{q_s + q_g} + \frac{(q_i q_g)^{0.5}}{q_i + q_g}\right] \tag{3}$$

Where q_i is the cloud ice mixing ratio, q_s the snow mixing ratio, and q_g the graupel mixing ratio, all in kg kg^{-1}.

2.4.1.2. Flash count calculation. Price and Rind (1992) developed a simple parameterization to simulate global lightning distributions. Separate lightning parameterizations were formulated for the two types of storms because of the difference in cloud characteristics between continental and maritime storms. Convective cloud top height is considered as the variable in both the cases. Continental parameterization is defined as,

$$F_c = 3.44 \times 10^{-5} H^{4.9} \tag{4}$$

and

$$w_c = 1.49 H^{1.09} \tag{5}$$

where, F_c is the continental flash frequency (flashes min^{-1}), H is the convective cloud top height and w_c is the maximum updraft intensity. Lightning parameterization for marine convective clouds follows a similar form, namely:

$$F_m = 6.4 \times 10^{-4} H^{1.73} \tag{6}$$

and

$$w_m = 2.86 H^{0.38} \tag{7}$$

The PR92 scheme also includes a direct empirical formulation between flash rate and maximum vertical velocity. This option wasn't used in our study.

2.4.2. WRF-ELEC model

Electric potential and total lightning flash rate are explicitly computed with WRF-ELEC (Fierro et al., 2013, available at: https://sourceforge.net/projects/wrfelec), an auxiliary package implemented in WRF. Mansell et al. (2005) included two kinds of in situ collisional charging processes known as inductive and non-inductive. An external electric field is required for the induction of charge of the colliding particles. As its name indicates, the non-inductive process doesn't require any external field. The non-inductive charge separation rate, parameterized in the Bulk Lightning Model (BLM) module of WRF-ELEC, follows (Mansell et al., 2005):

$$\frac{\partial \rho_{xy}}{\partial t} = \beta \delta q_{xy}\left(1 - E_{xy}\right) E_{xy}^{-1}\left(n_{xacy}\right) \tag{8}$$

where ρ_{xy} is the density (Cm^{-3}) of charge separated through the collision between hydrometeors of x and y, δq_{xy} is the weighted average of the separated charge (C) per rebounding collision between hydrometeors of x and y, β is an arbitrary factor that limits charging at low temperatures, n_{xacy} is the number concentration collection rate integral, E_{xy} is the collection efficiency, and δq is the magnitude of charge separated within a grid cell determined from a polynomial fit to the non-inductive critical charging curve. The parameterization of δq is as follows (Mansell et al., 2005; Saunders et al., 1991):

$$\delta q = B D_I^a \left(V_g - V_I\right)^b q(RAR) \tag{9}$$

where B, a, and b are a function of crystal size (Table 1 in Mansell et al., 2005); $D_I$is the mean volume diameter of the ice crystal–snow, V_g and V_I are the mass- weighted mean terminal fall speeds for graupel and cloud ice (or snow), respectively; $q(RAR)$ is the charge separation as a function of the Riming Accretion Rate (RAR) from Brooks et al. (1997), later modified by Mansell et al. (2005). The RAR at which the charge obtained

Table 1
Configurations used in WRF-ARW and WRF-ELEC simulations.

Parameters	Configurations
DX, DY	9 km, 3 km
NX × NY	120 × 120 (d01) 178 × 244 (d02)
NZ	34
Microphysics scheme	NSSL 2-moment (Mansell et al., 2010)
Cumulus physics	Grell 3D (Grell, 1993) (d01) No cumulus (d02)
Boundary layer scheme	Yonsei University scheme (YSU) (Hong et al., 2006)
Land surface model	Noah
Radiation	RRTMG

by graupel changes its sign is defined by the critical *RAR* curve parameterized based on the work of Saunders and Peck (1998). The critical *RAR* curve, as a function of temperature (°*C*), is defined as follows:

$$RAR_{crit} = \begin{cases} s(T) : T > -23.7\ C \\ k(T) : -23.7^{\circ} > T > -40^{\circ} C \\ 0 : T \leq -40\ C \end{cases} \quad (10)$$

where, the functions of $s(T)$ and $k(T)$ are given below as (Saunders and Peck, 1998):

$$s(T) = 1 + 7.9262 \times 10^{-2} T + 4.4847 \times 10^{-2} T^2 + 7.4754 \times 10^{-3} T^3 + 5.4686 \times 10^{-4} T^4 + 1.6737 \times 10^{-5} T^5 + 1.7613 \times 10^{-7} T^6 \quad (11)$$

and

$$k(T) = 3.4\left[1 - \left(\frac{|T + 23.7|}{-23.7 + 40}\right)^3\right] \quad (12)$$

The positive charge ($RAR > RAR_{crit}$) and negative charge ($0.1\ gm^{-2} \ll RAR_{crit}$) of graupel are calculated as follows (Saunders and Peck, 1998):

$$q_{+}(RAR) = 6.74(RAR - RAR_{crit}) \quad (13)$$

$$q_{-}(RAR) = 3.9(RAR_{crit} - 0.1) \times \left(4 \times \left[\frac{RAR - (RAR_{crit} + 0.1)/2}{RAR_{crit} - 0.1}\right]^2 - 1\right) \quad (14)$$

Brooks and Saunders (1994) stated that inductive or polarization charging could be, in some circumstances, non-negligible where a strong electric field is present. Hence, the inductive electrification is also implemented in WRF-ELEC following the parameterization of Ziegler et al. (1991). The inductive charging rate is a function of the mean cosine of the angle of rebounding collision, the rebound probability, and the vertical component of the electric field. Due to the minimal conductivity of the ice and the relatively short collision time, the ice-ice collisions are neglected in inductive charging (Gaskell, 1981). Therefore, only the collisions between cloud water (with subscript *c*) and ice-graupel-hail (with subscript *g*) are considered in our study according to Mansell et al. (2005):

$$\frac{\partial \rho_g}{\partial t} = \frac{\pi^3}{8}\left[\frac{6\overline{V_g}}{\Gamma(4.5)}\right] E_{gc} E_r n_{t,c} n_{0,g} D_c^2 \left[\pi \Gamma(3.5) \varepsilon < cos\theta > E_z D_{n,g}^2 - \frac{\Gamma(1.5)\rho_g}{3 n_{t,g}}\right] \quad (15)$$

where, ρ_g is the charge density carried by the graupels; D_c is the mean diameter of the cloud droplets; E_{gc} is the collision efficiency between the graupels and cloud water droplets; E_r is the rebound probability; $n_{t,c}$ and $n_{0,g}$ are the total cloud water and the graupel number density, respectively; $\overline{V_g}$ is the mass-weighted mean fall speed of graupels; $\Gamma(x)$ is the complete gamma function; $D_{n,g}$ is the characteristic diameter of graupel (reciprocal of the slope parameter); $n_{0,g}$ is the number concentration intercept of graupel; $<cos\theta>$ is the mean cosine of the angle of rebounding collision; E_z is the vertical component of the electric field; and ε is the electrical permittivity of air.

After computing grid cell non-inductive and inductive charging rates, their sum is then calculated for every predicted hydrometeor species. The law of conservation of total charge has been taken into account during charge transfer occurring during mass exchange between each hydrometeor species. According to Fierro et al. (2013), charges carried by precipitating particles pass through the lower boundary and eventually leave the domain. Eventually, the total charge density on each charge species is calculated from the sum of all charge production rate terms and mass transfer plus the charge density calculated at the previous time step. Then the BoxMG electric potential solver, implemented in WRF-ELEC, computes the electric potential by solving the 3D Poisson equation using Dirichlet boundary conditions for vertical boundaries and Neumann boundary conditions for lateral boundaries (Mansell et al., 2005):

$$\nabla^2 V = -\frac{\rho_{tot}}{\varepsilon_o} \quad (16)$$

Where, V is the electric potential, ε_o is the electrical permittivity of air and ρ_{tot} is the total volume charge density. After solving the Poisson equation, the three components of the electric field can be retrieved from the following equation,

$$\boldsymbol{E} = -\nabla V \quad (17)$$

2.4.2.1. The discharge model. The discharge model in WRF-ELEC

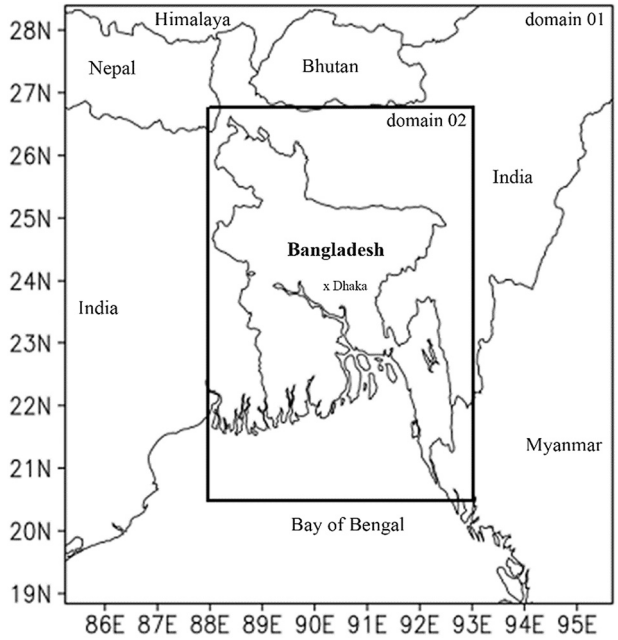

Fig. 1. Model domains (one nested). Both domains are centered at lat = 23.70° N and lon = 90.46° E over Dhaka.

follows the parameterization of Ziegler and MacGorman (1994) and MacGorman et al. (2001). In this model, lightning initiation occurs at grid points where the electric field exceeds the critical breakdown value of 120 kVm^{-1} (consistent with the break-even field magnitude defined by Gurevich et al., 1992). A cylinder of fixed radius R, extending throughout the entire depth of the domain, is centered on each initiation point upon discharge. In cloud-based simulations, this radius is usually set to 6 km (as in Fierro et al., 2013).

2.4.3. Model setup

In the present study, fifteen simulations were conducted for five lightning cases using two domains (one of which nested) (Fig. 1): Ten out of these fifteen simulations used the original WRF-ARW model (i.e., five using the LPI scheme and five using Price and Rind, 1992, hereafter PR92) and the remaining five used WRF-ELEC. Every simulation is initialized at 0000 UTC on the day of the event and is integrated for 24 h. The physical parameterizations and model configuration of WRF-ARW and WRF-ELEC are listed in Table 1.

For consistency, the NSSL two-moment microphysics scheme (Mansell et al., 2010) was used to parameterize microphysical processes in all fifteen simulations. Rationale for this choice is that the electrification in WRF-ELEC is currently tied to the NSSL 2-moment microphysics scheme. The NSSL scheme predicts the mass mixing ratio and concentration for raindrops, ice crystals, cloud droplets, snow, hail and graupel. The PR92 lightning prediction scheme, which bases its algorithm on the level of neutral buoyancy from a convective parameterization, is used to calculate lightning flashes. The cloud-top adjusted parameter in PR92 is set to the default value of 2 km (following Wong et al. (2013) and Mohan et al. (2021)).

For the WRF-ELEC runs, both inductive and non-inductive charging are considered and are coupled with the bulk lightning discharge scheme of Ziegler and MacGorman (1994). The NSSL screening layer scheme based on Ziegler et al. (1991) was activated and the height-varying vertical profile of Dwyer (2003) was used for lightning initiation threshold. Similar to Fierro et al. (2013), a discharge cylinder with a 6-km radius was used. Upon discharge, 30% of the total charge is assumed to be neutralized by superposition onto the carriers of opposite charge.

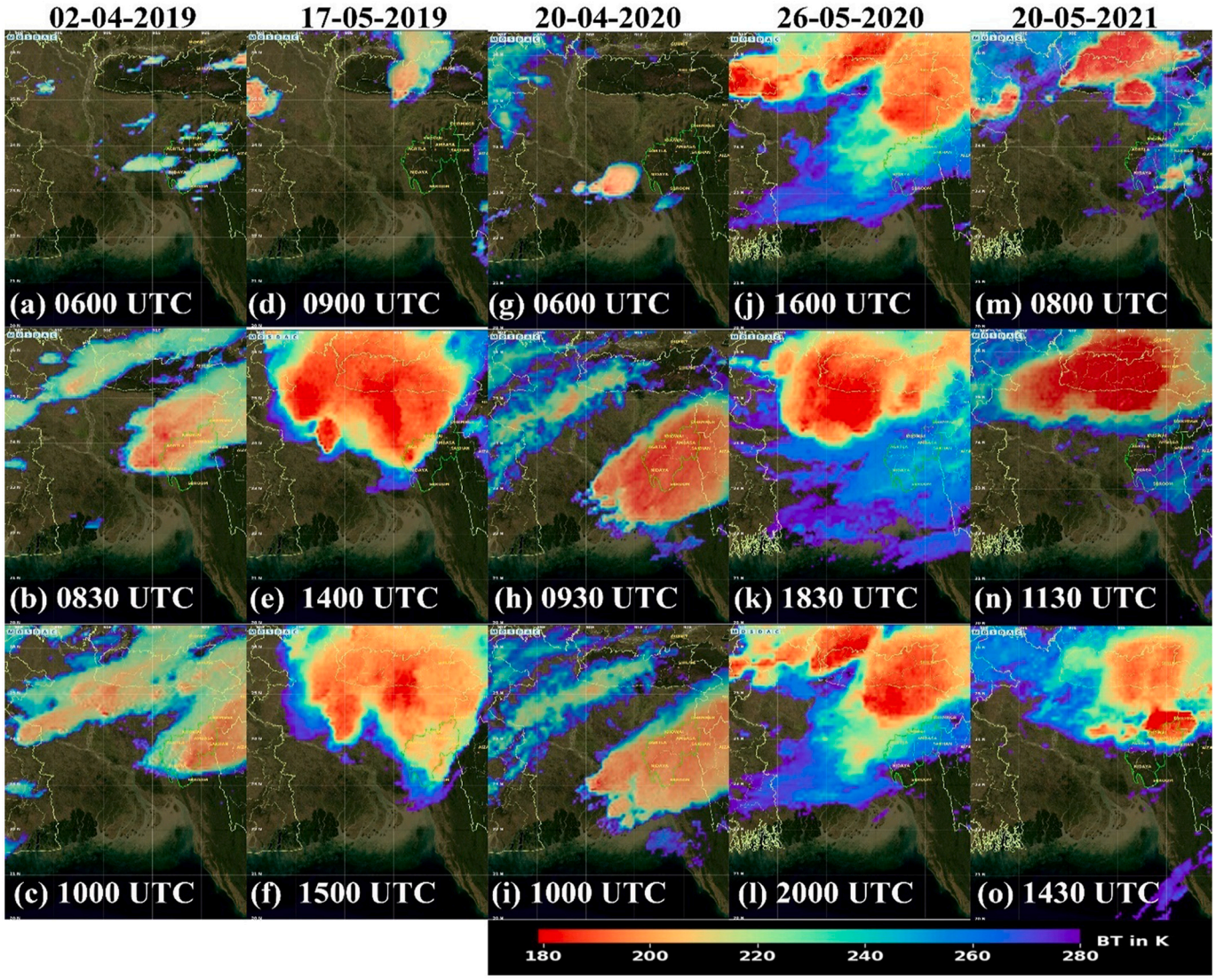

Fig. 2. INSAT-3DR satellite-derived visible TIR-1 blended brightness temperature images representing cloud coverage of the five lightning cases of the present study. Labels a, d, g, j, m represent the initial stage of convective cells. Similarly, b, e, h, k, n represent the mature stage and c, f, i, l, o the cloud conditions during the dissipation stage.

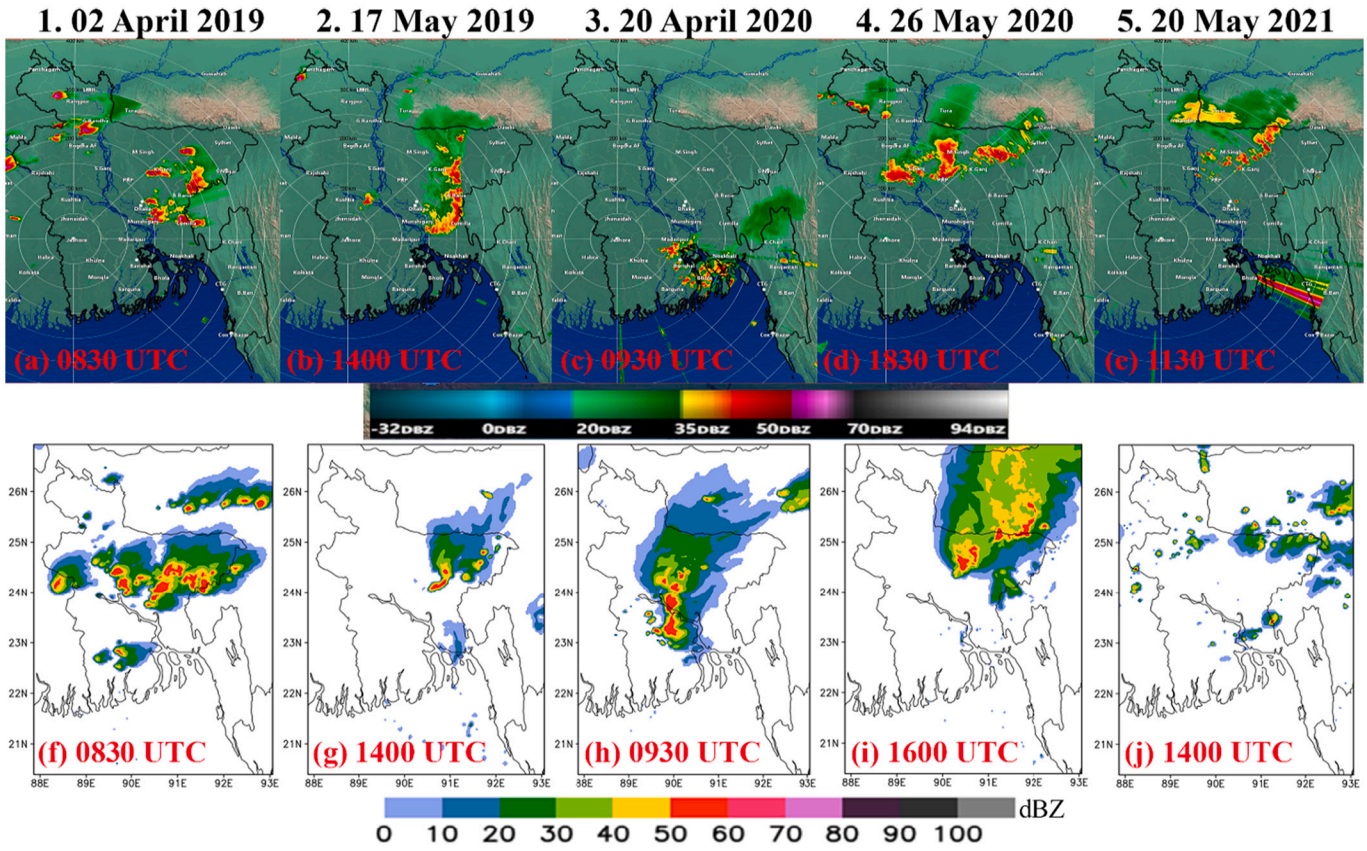

Fig. 3. The composite (column maximum) reflectivity (dBZ) from the MTR-DWR (a–e) and the WRF model (f–j) for the five cases analyzed in this study at the time of their respective mature stages.

3. Results and discussion

3.1. Precipitation structure

A meteorological satellite can be used to monitor cloud systems associated with deep, mixed-phased convection. The half-hourly visible (VIS) channel (0.65 μm) and thermal infrared (TIR) channel (10.8 μm) data from the INSAT-3D satellite were used in the present study to track the life-cycle of the storms in the simulation domain based on the cloud-top brightness temperatures (Fig. 2). The simulated composite (column maximum) reflectivity was also analyzed during the mature stage and compared against local radar observation for all cases herein (Fig. 3).

On 02 April 2019, two organized convective cells with a minimum brightness temperature (BT) of around 220 K were identified at 0600 UTC over the central part of Bangladesh (Fig. 2a). These two cells later intensified and merged at around 0800 UTC. A mature thunderstorm complex formed at 0830 UTC with 190 K BT covering the central and eastern parts of Bangladesh (Fig. 2b). The MTR-DWR also showed several echoes nearing 55 dBZ over the region at 0830 UTC (Fig. 3a). The model was able to simulate the storm system at the same time as the observations but with maximum reflectivity values near 70 dB*Z* (Fig. 3f). At around 1000 UTC, the storm complex propagated towards the south-westward direction and started to dissipate (Fig. 2c). A similar storm system occurred on 20 April 2020 (Fig. 2g, h, i). The DWR captured the system, which was associated with maximum reflectivity values of about 50 dB*Z* (at 0930 UTC Fig. 3c). The model simulated the event at the right time with some spurious echoes over the central portion of the country (Fig. 3h). On 17 May 2019, two convective cells occurred at around 0900 UTC over the northern parts of the country (Fig. 3d). These storms eventually merged, and grew upscale into a mesoscale convective system (MCS) associated with 180 K BT (at 1400 UTC) covering a large portion of Bangladesh, including Dhaka. The simulated reflectivity at the time (1400 UTC) reached 50 dB*Z* with an overall smaller spatial coverage over the region. The storms began to dissipate at 1500 UTC (Fig. 2f). For the fourth case considered herein on 26 May 2020, several convective systems developed over the northern portion of the country at around 1600 UTC (Fig. 2j). This complex of discrete storms propagated eastward while growing upscale into a mesoscale convective system (MCS) covering most of the central and northern regions of the country (Fig. 2k). The last case on 20 May 2021 shows more discrete cells over the same general area as case 4, which the model failed to simulate well in terms of intensity and timing. The simulations reveal temporal shifts/biases in convection initiation for the fourth (02:30 h earlier) and fifth cases (2 h later). Overall, however, the model simulated spatial coverage of the storms reasonably well albeit with occasional spurious echoes (Fig. 3d, e, i, j). Almost similar cloud-top BT characteristics were observed for thunderstorms over this region by Rabbani et al. (2021) and Goyal et al. (2016).

The 24-h accumulated simulated rainfall and NASA GPM (IMERG) rainfall estimates were used to evaluate precipitation structure for each of the five cases herein (Fig. 4). The model simulated reasonably similar spatial precipitation patterns as the GPM observations for cases 1, 2 and 5. Fig. 4, however, also reveals many areas where rainfall was either over- or underestimated by the model. The southern part of the country received a maximum of 60 mm accumulated rainfall on 20 April 2020 (Fig. 4f), which the model failed to simulate (Fig. 4e). It also failed to capture the heavy rainfall over the northern part of the country on 26 May 2020 (Fig. 4g, h). Along with the qualitative comparison, time series of neighborhood score metrics such as Equitable Threat Score (ETS) and Fraction Skill Score (FSS) for three neighborhood radii (1*dx, 3*dx and 5*dx where dx = 3 km) and for three precipitation thresholds (2.5, 5 and 10 mm h^{-1}) were analyzed (Fig. 5). The contingency table elements

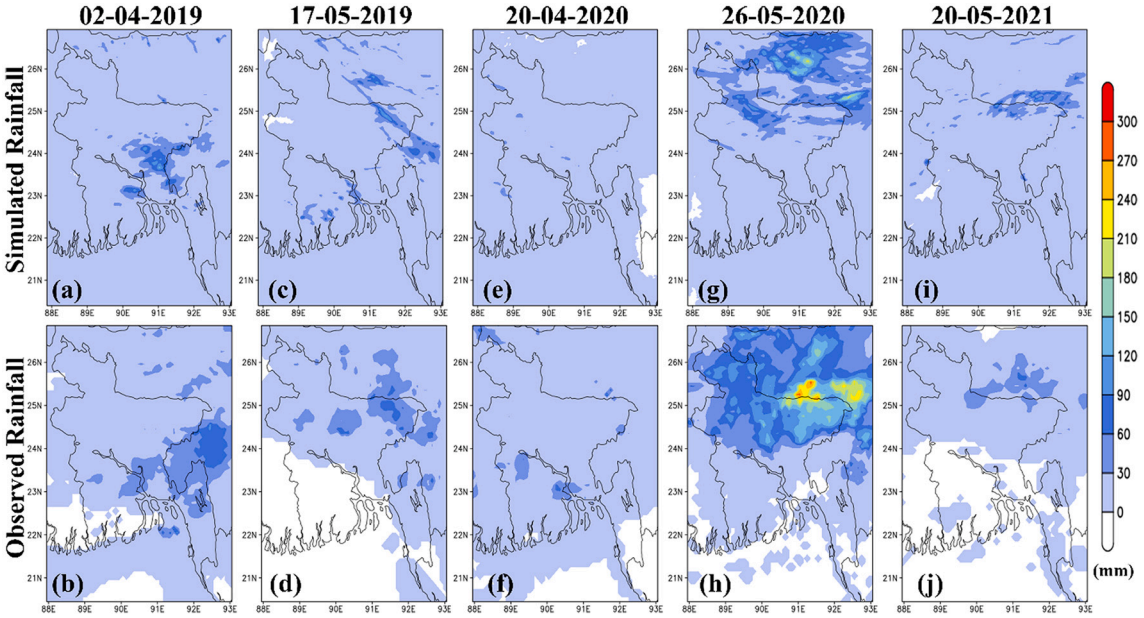

Fig. 4. Comparison of 24-h accumulated simulated rainfall (a,c,e,g,i) with NASA GPM IMERG rainfall (b,d,f,h,j).

were computed by taking the hourly forecast outputs from the model and the observed rainfall products from NASA's GPM multi-satellite precipitation dataset. The neighborhood methods are preferable because they partially alleviate the "double penalty" events associated with small displacement errors in the model (e.g., Fierro et al., 2015). The ETS (Mason, 2003) estimates the fraction of observed and/or forecasted rainfall events that were correctly forecasted and adjusted for hits associated with a random prediction, where the predicted occurrence or non-occurrence is independent of observation or non-observation (Comellas Prat et al., 2021). The FSS (Roberts and Lean, 2008) is a neighborhood spatial validation method used particularly for precipitation verification that directly compares the fractional coverage of events over time windows centered on the forecasts and observations (Skok and Roberts, 2016).

The ETS and FSS in Fig. 5 indicate that the forecast rainfall for all cases is predicted overall reasonably well. The third case shows the lowest ETS (−0.1) and FSS (0.25) values that may be attributed to the spurious precipitation pattern over the central part of the country discussed earlier (Fig. 5e and f). As the neighborhood radius increases, the FSS increases significantly as expected, especially for lower precipitation thresholds (5b, 5d, 5f, 5 h and 5j). If the precipitation thresholds increase, both ETS and FSS values decrease. In terms of both ETS and FSS, the rainfall threshold of 2.5 mm along with the neighborhood radius of 15 km produces the best results for each case.

Performance diagrams (Roebber, 2009) were also constructed for each case to visualize more concisely the statistical skill scores for aforementioned rainfall thresholds and neighborhood radii against observational data (Fig. 6). In this particular diagram, four forecast evaluation metrics are conveniently merged: 1) False Alarm Ratio (FAR) which is conditioned on predicted events, 2) Probability of Detection (POD) which is conditioned on observed events, 3) Critical Success Index (CSI), which is a function of both POD and FAR, and 4) Frequency Bias (FBIAS) which provides a measure of the ratio of predicted events to observed events. A simulation is considered to be performing optimally when its corresponding symbol is located closest to the upper right-hand corner. The results of the diagrams (Fig. 6a, b, c and e) reveal that those simulations with the rainfall threshold of 2.5 mm and the neighborhood radius of 15 km perform overall best (consistent with the earlier ETS analysis). As expected, using a higher neighborhood radius improves the probability of detection, which for our cases is more marked for the lower precipitation thresholds. The success ratio also improves with increasing radius but appears to be more sensitive to the precipitation thresholds.

From these diagrams, it can also be seen, again, that the third case does not perform well at 10 mm (Fig. 6c and e). One apparent feature of the diagrams is that nearly all of simulations show increasing biases along with lower success ratios for the increasing rainfall thresholds. This indicates that, for convective rainfall, the model systematically produces high FAR and low POD.

3.2. *Lightning activity*

For all cases, the spatial distributions of the simulated lightning flash counts are analyzed and validated against the observations from LIS flash lightning activity. As the LIS has short temporal (approximately 1–3 min for the studied cases) and spatial coverage, the lightning flash counts by the LIS and the simulations are normalized by dividing the flash count by the maximum value in the domain. Due to the limitation of the LIS observations, the qualitative analyses primarily focus on the spatial patterns of the lightning activity in lieu of their actual flash rates. The spatial distribution of LIS flash lightning activity and simulated flash counts and the LPI are presented in Fig. 7–11. The LPI is studied and shown herein for identifying regions of lightning activity.

The lightning activity that occurred on 02 April 2019 is considered first. LIS detected lightning activity over the central and northern areas of the country (Fig. 7a). The LPI detected similar lightning prone areas (Fig. 7d) but missed the lightning activity over the northern areas. The spatial pattern of the simulated lightning flashes by WRF-ELEC are overall consistent with the LIS observations (Fig. 7c). PR92 fails to capture the location of lightning flashes (compared to LIS observations) and also produces spurious flashes in the northern portions of the domain (Fig. 7b). Choudhury et al. (2020) also estimated normalized lightning flashes with PR92 and found that the simulated flashes were overall comparable with those detected by LIS.

For the case of 17 May 2019, the lightning activity observed by LIS is mostly concentrated over the central-eastern part of the country (Fig. 8a). LPI was able to predict the main areas of lightning occurrence with respect to the LIS observations whereas WRF-ELEC suffers from a notable spatial displacement error (Fig. 8c and d). The locations of the lightning flashes diagnosed by PR92 are overall consistent with the

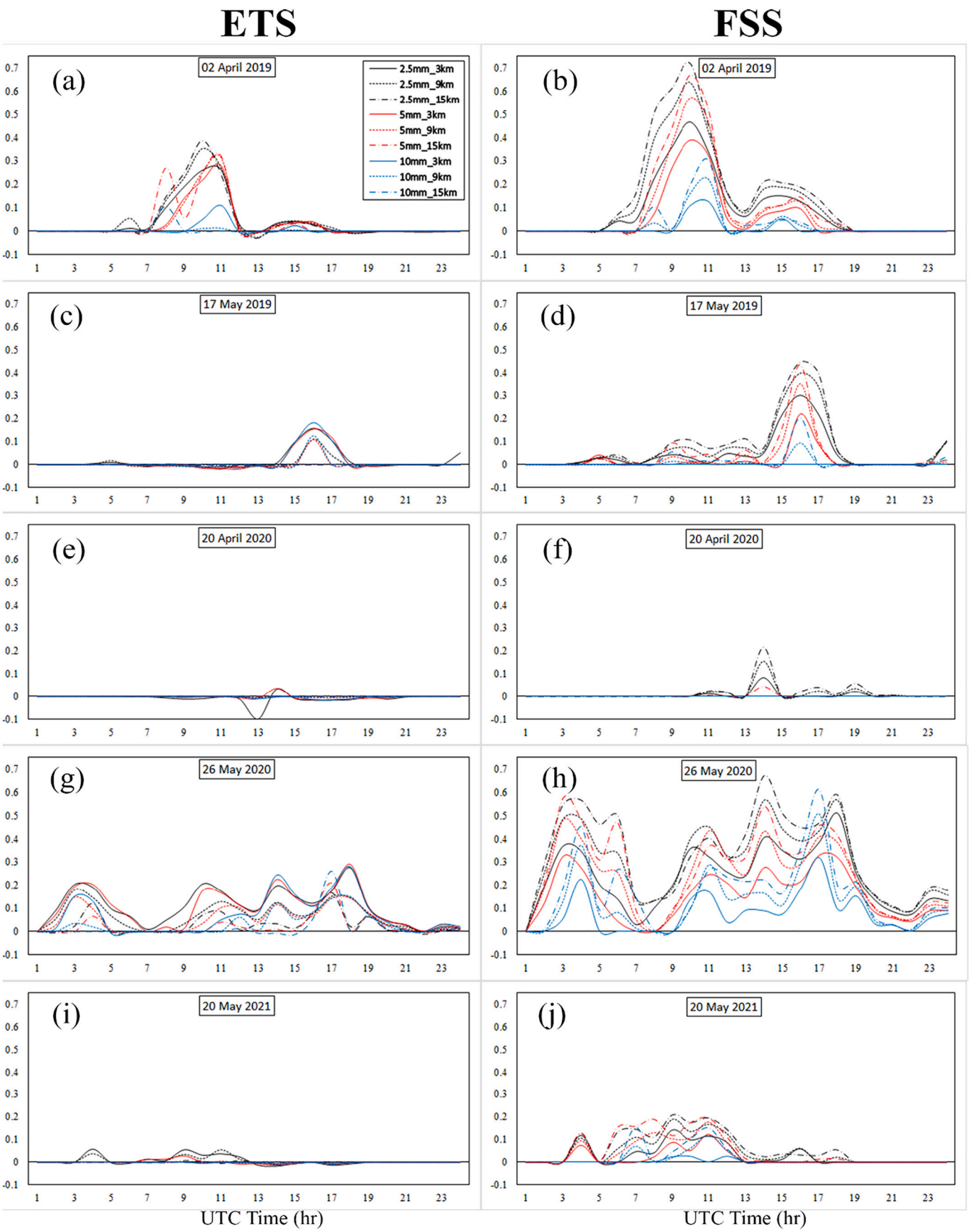

Fig. 5. Time series of ETS and FSS for three neighborhood radii (3 km, 9 km and 15 km) and for three thresholds (2.5, 5 and 10 mm h^{-1}) of hourly rainfall of all five cases: 02 April 2019 (a, b), 17 May 2019 (c,d), 20 April 2020 (e, f), 26 May 2020 (g, h) and 20 May 2021 (i, j).

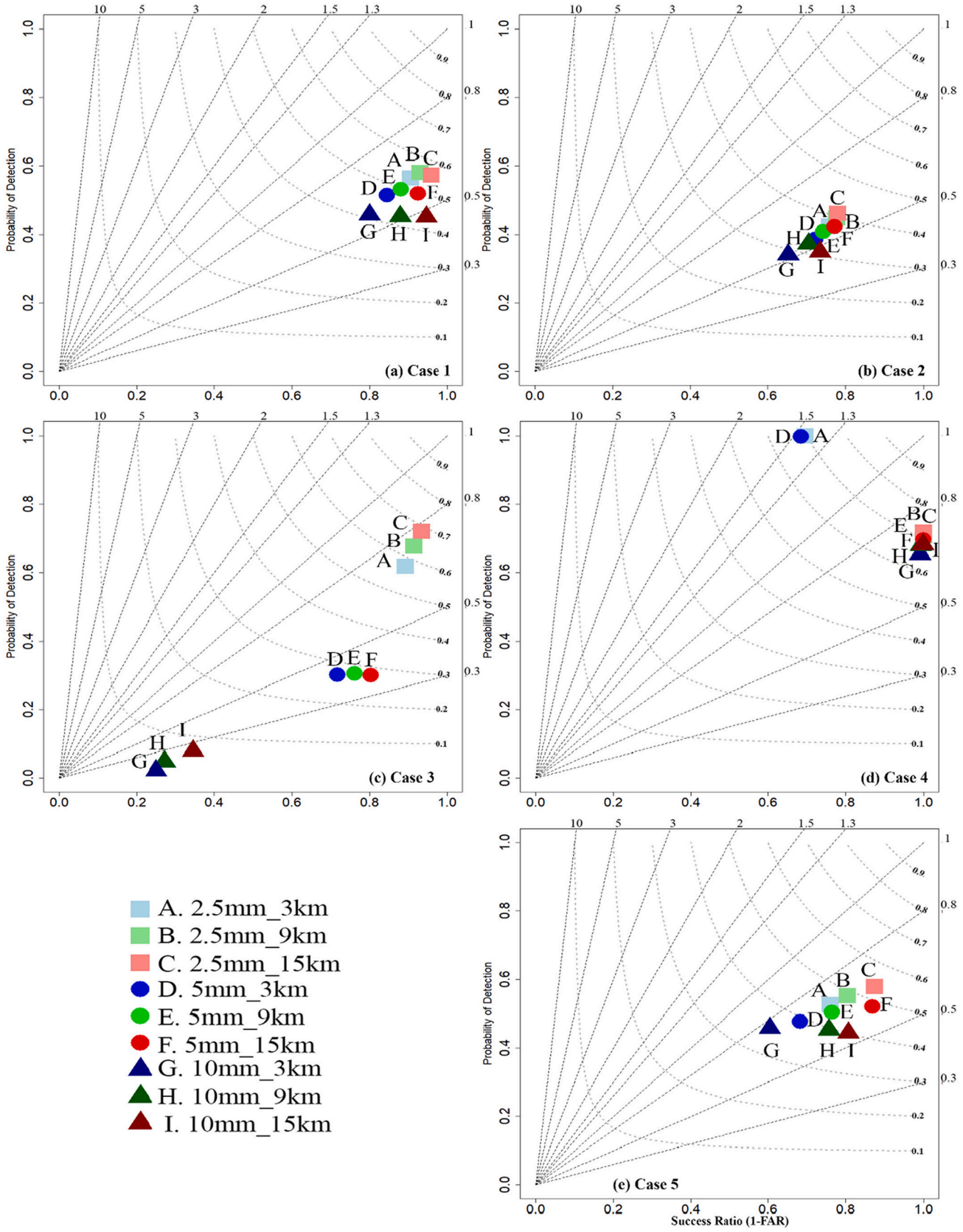

Fig. 6. Roebber (2009) performance diagram for all simulations. Light to dark shaded blue, green and red represents 3 km, 9 km and 15 km nearest neighborhood radii respectively. The square, circle and triangle symbols represent 2.5 mm, 5 mm and 10 mm rainfall thresholds, respectively. Dashed lines show the frequency bias and the curved lines represent the CSI. (For interpretation of the references to colour in this figure legend, the reader is referred to the web version of this article.)

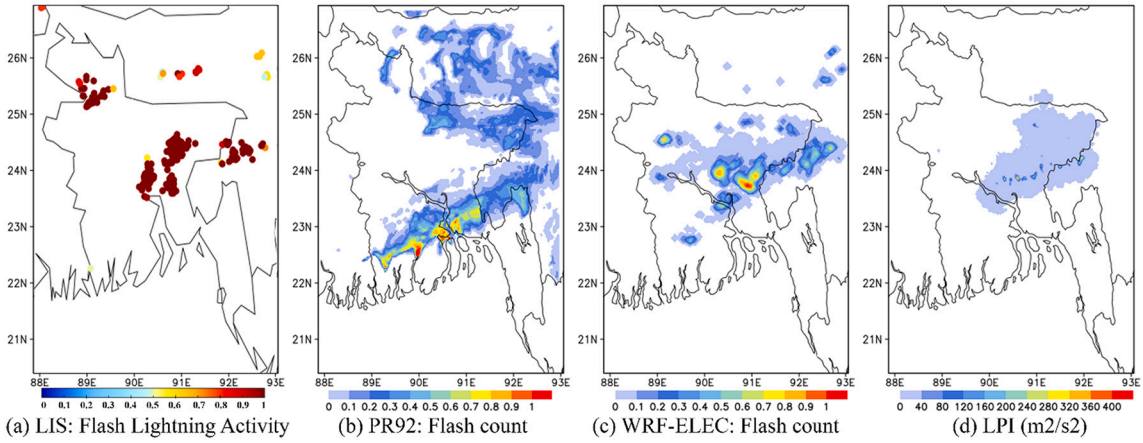

Fig. 7. (a) The spatial distribution of normalized LIS flash lightning activity on 02 April 2019 during 07:53:54 to 07:56:20 UTC over the simulation domain. The simulated lightning activity based on (b) PR92 lightning flash counts (IC + CG) accumulated between 0730 and 0830 UTC, (c) WRF-ELEC estimated flash count accumulated between 0730 and 0830 UTC, and (d) LPI (m^2s^{-2}) at 0800 UTC. The simulated flashes are normalized and estimated from the innermost 3-km domain.

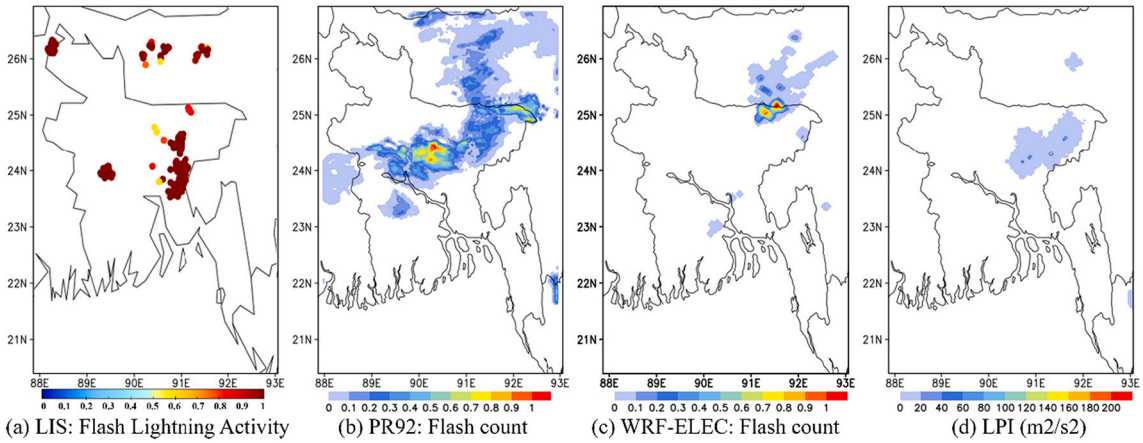

Fig. 8. (a) The spatial distribution of normalized LIS flash lightning activity on 17 May 2019 during 13:52:47 to 13:53:54 UTC. The simulated lightning activity based on (b) PR92 lightning flash counts (IC + CG) accumulated between 1330 and 1430 UTC, (c) WRF-ELEC estimated flash count accumulated between 1330 and 1430 UTC, and (d) LPI (m^2s^{-2}) at 1400 UTC.

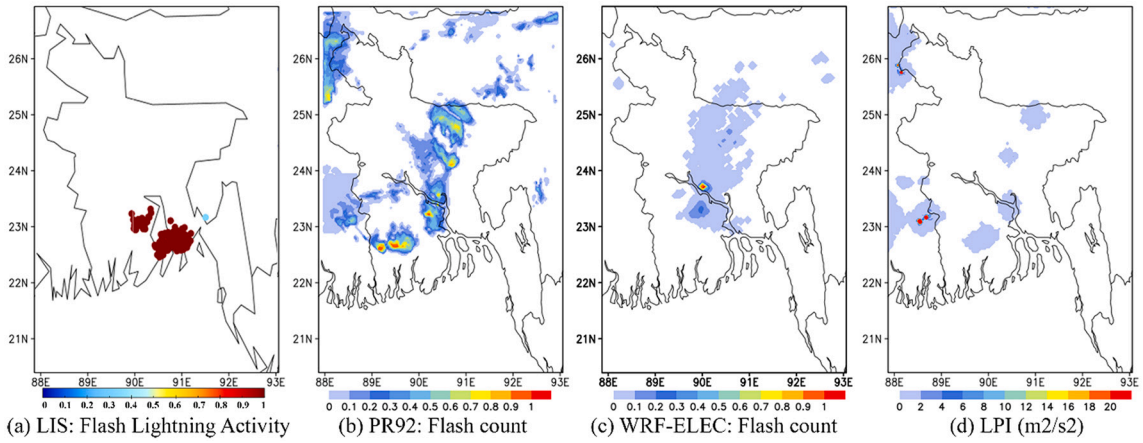

Fig. 9. (a) The spatial distribution of normalized LIS flash lightning activity on 20 April 2020 during 09:13:18 to 09:13:42 UTC. The simulated lightning activity based on (b) PR92 lightning flash counts (IC + CG) accumulated between 0900 and 1000 UTC, (c) WRF-ELEC estimated flash count accumulated between 0900 and 1000 UTC, and (d) LPI (m^2s^{-2}) at 0930 UTC.

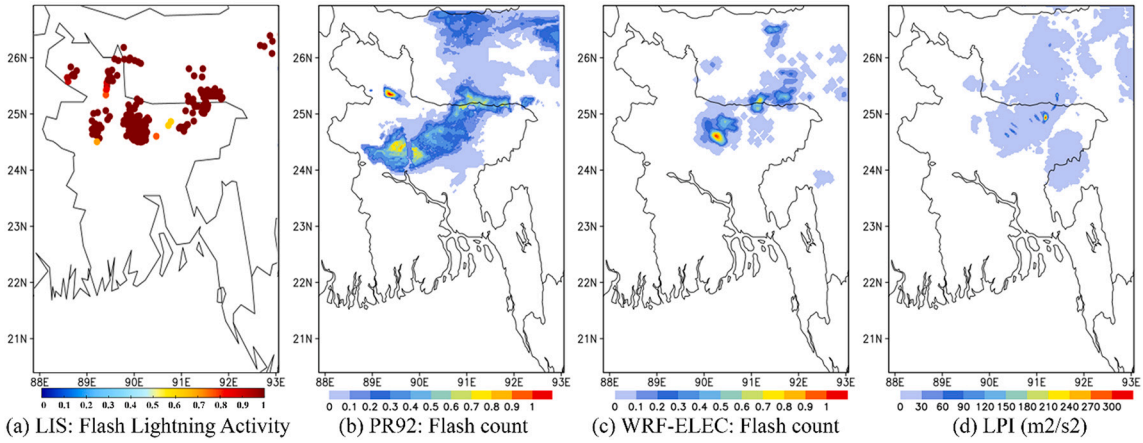

Fig. 10. (a) The spatial distribution of normalized LIS flash lightning activity on 26 May 2020 at 18:16:22 to 18:17:31 UTC. The simulated lightning activity based on (b) PR92 lightning flash counts (IC + CG) accumulated between 1530 and 1630 UTC, (c) WRF-ELEC estimated flash count accumulated between 1530 and 1630 UTC, and (d) LPI (m^2s^{-2}) at 1600 UTC.

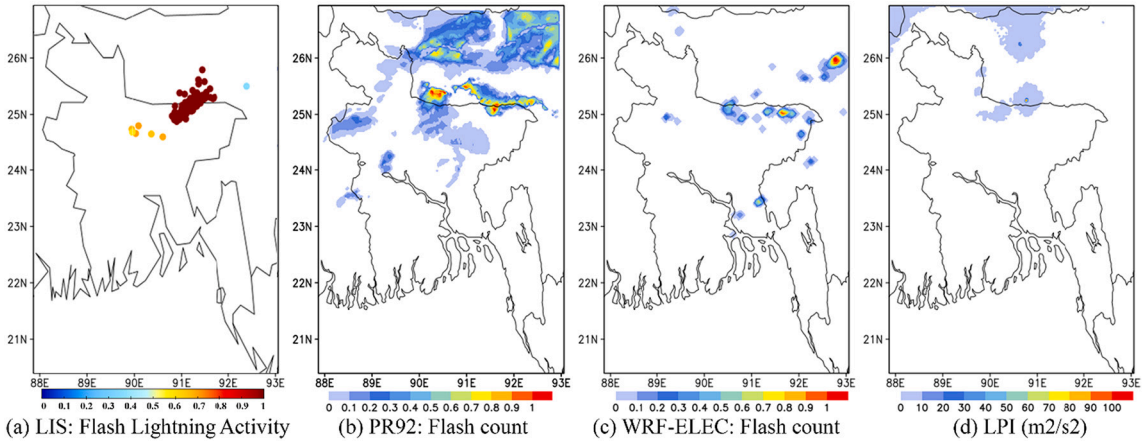

Fig. 11. (a) The spatial distribution of normalized LIS flash lightning activity on 20 May 2021 at 11:27:46 to 11:29:46 UTC. The simulated lightning activity based on (b) PR92 lightning flash counts (IC + CG) accumulated between 1300 and 1400 UTC, (c) WRF-ELEC estimated flash count accumulated between 1300 and 1400 UTC, and (d) LPI (m^2s^{-2}) at 1400 UTC.

observations (Fig. 8d). For this specific case, the WRF-ELEC simulated lightning flashes do not cover all areas of observed lightning activity (Fig. 8f). Mohan et al. (2021) evaluated different lightning parameterization schemes and showed that, for four cases, the LPI and PR92 based lightning parameterization were able to reasonably reproduce the observed lightning activity over Maharashtra in the western and central part of India.

LIS showed lightning activity for the third case on 20 April 2020 at around 0913 UTC (Fig. 9a). The lightning spatial pattern predicted by the LPI is not thoroughly consistent with the LIS observation (Fig. 9d). Model simulated lightning flashes predicted by PR92 and WRF-ELEC also show different patterns with respect to the LIS observations.

Shifting gears to the results for the fourth case on 26 May 2020, the main regions of lightning activity are predicted rather well by LPI (Fig. 10d) where LIS showed lightning activity over the northern portions of the country (Fig. 10a). The simulated flashes are also consistent with the LIS observations (Fig. 10b and c). Despite these positive attributes, the model captured the storms and, hence, lightning activity two hours thirty minutes earlier than observed.

The last case investigated, 20 May 2021, covers the northern areas of the country as well. All of the predicted spatial distribution of LPI (Fig. 11d) and lightning flashes (Fig. 11b and c) estimated by both the PR92 and the WRF-ELEC are overall consistent with the LIS-observed lightning activity (Fig. 11a). Akin to the fourth case, however, the simulated lightning suffers from a temporal shift but two hours later relative to the observations. These deviations may arise either from model error or from the usage of global forecast datasets to derive the initial and boundary conditions (Goines and Kennedy, 2018).

The performance of the LPI and the lightning flashes simulated by WRF model in all cases of this study are overall reasonably consistent with the previous results of Dementyeva et al. (2015), Lagasio et al. (2017) and Fiori et al. (2016) for different regions. Gharaylou et al. (2019) showed similar results for Iran in predicting lightning activity based on WRF-ELEC.

4. Conclusion

Lightning related hazards are a global concern for life and property, as they may occur at any instant, at any location worldwide. Owing to its noteworthy economic impact, heightened emphasis has been directed by the scientific community in the last two decades toward improving lightning forecasting systems using state-of-the-art numerical weather prediction models. In Asia, Bangladesh also faces significant damages and threats due to lightning for which numerical prediction studies are warranted to help develop better mitigation policies and to minimize the detrimental socioeconomical impacts of lightning. The present study analyzed five high impact lightning cases that occurred in Bangladesh using DWR, satellite-based observations and the community, multi-scale

WRF-ARW model. This evaluation makes use of two diagnostic lightning prediction methods (LPI and PR92) and an explicit, physics-based approach from cloud electrification referred to as WRF-ELEC.

The simulated spatial pattern of lightning activity was overall consistent with the LIS observations. The WRF-ARW results show temporal and spatial displacement errors in some of the cases in addition to producing spurious echoes and lightning in the domain. Other than model error, storm electrification is complex and requires several assumptions to account for some of the unobservable processes associated with lightning such as in-cloud charging and breakdown (Mansell et al., 2005). Akin to other statistical approaches, the PR92 lightning prediction scheme assumes that lightning flash count depends on spatial and temporal averages of parameters derived from the model fields. Such an assumption introduces potential errors in forecasting lightning flash count because convective clouds develop over different time scales and propagate at different speeds depending on the existing environmental conditions. The present study shows that, overall, the simulated lightning fields for all five cases are in reasonable agreement with the available satellite observations from LIS. WRF-ELEC based simulations slightly overperform PR92 and LPI in four of the five cases. Thus, given comparable computational costs, we would recommend WRF-ELEC over the two other schemes for operational usage.

As a final note, potential future research works would include the usage of lightning data assimilation to potentially address the timing and location of the convection and, ultimately, help improve lightning and short-term rainfall forecasts (Comellas Prat et al., 2021; Fierro et al., 2015, 2012). Reducing the horizontal grid spacing from 3-km herein down to cloud-resolving scales (1 km) would also be warranted to investigate. Rigorous sensitivity studies should also be conducted with the help of ground and satellite-based observations to potentially help improve these results further. The present study is one of the first attempts to simulate lightning activity explicitly over Bangladesh. As lightning-related fatalities are increasing in the country, the present study may help authorities of public policy and operational forecasting institutions to implement an effective lightning prediction system that can save lives and properties and improve the safety of rural, fishing and farming communities.

Credit authorship contribution statement

Khan MD Golam Rabbani: Conceptualization, Data curation, Methodology, Software, Validation, Formal analysis, Investigation, Resources, Writing - original draft, Writing - review & editing, Visualization, Funding acquisition. **Md. Jafrul Islam:** Conceptualization, Methodology, Formal analysis, Investigation, Writing - original draft, Writing - review & editing, Validation. **Alexandre O. Fierro:** Conceptualization, Supervision, Formal analysis, Writing - original draft, Writing - review & editing, Validation. **Edward R. Mansell:** Conceptualization, Supervision, Software, Formal analysis, Writing - original draft, Writing - review & editing, Validation. **Pappu Paul:** Writing - original draft, Funding acquisition.

Declaration of Competing Interest

The authors declare that they have no known competing financial interests or personal relationships that could have appeared to influence the work reported in this paper.

Acknowledgment

This work was mostly funded by the Bangladesh Climate Change Trust (BCCT), under the project entitled 'Investigation of Meteorological Conditions relating to Lightning and Development of Resilient Communities in Lightning Prone Areas in Bangladesh' which is implemented by the Department of Meteorology, University of Dhaka'. The authors also acknowledge the Department of Meteorology, University of Dhaka for providing additional funding and allowing the use of the laboratory facilities to perform the research. Funding for Dr. Alex Fierro was provided by NOAA/Office of Oceanic and Atmospheric Research under NOAA-University of Oklahoma Cooperative Agreement #NA11OAR4320072, U.S. Department of Commerce.

References

Ackerman, S., Knox, J., 2012. Meteorology: Understanding the Atmosphere. Jones & Bartlett Publishers.

Ahasan, M.N., Quadir, D.A., Khan, K.A., Haque, M.S., 2015. Simulation of a Thunderstorm event over Bangladesh using WRF-ARW Model. J. Mech. Eng. 44, 124–131. https://doi.org/10.3329/jme.v44i2.21437.

Al-Amin Hoque, M., Billah, Md.M., Pradhan, B., 2019. Spatio-temporal and demographic distribution of lightning related casualties in northeastern part of Bangladesh. Int. J. Disaster Risk Reduct. 38, 101197 https://doi.org/10.1016/j.ijdrr.2019.101197.

Albrecht, R.I., Goodman, S.J., Buechler, D.E., Blakeslee, R.J., Christian, H.J., 2016. Where are the lightning hotspots on Earth? Bull. Am. Meteorol. Soc. 97, 2051–2068. https://doi.org/10.1175/BAMS-D-14-00193.1.

Barthe, C., Deierling, W., Barth, M.C., 2010. Estimation of total lightning from various storm parameters: a cloud-resolving model study. J. Geophys. Res.-Atmos. 115 https://doi.org/10.1029/2010JD014405.

Blakeslee, R.J., 2020. Quality Controlled Lightning Imaging Sensor (LIS) on International Space Station (ISS) Science Data. Huntsville, AL, USA, NASA Global Hydrology Resource Center DAAC. https://doi.org/10.5067/LIS/ISSLIS/DATA108.

Bright, D.R., Wandishin, M.S., Jewell, R.E., Weiss, S.J., 2005. A Physically Based Parameter for Lightning Prediction and its Calibration in Ensemble Forecasts. In: Preprints, Conf. On Meteor. Appl. Of Lightning Data, Amer. Meteor. Soc., San Diego, CA. Citeseer, p. 30.

Brooks, I.M., Saunders, C.P.R., 1994. An experimental investigation of the inductive mechanism of thunderstorm electrification. J. Geophys. Res.-Atmos. 99, 10627–10632. https://doi.org/10.1029/93JD01574.

Brooks, I.M., Saunders, C.P.R., Mitzeva, R.P., Peck, S.L., 1997. The effect on thunderstorm charging of the rate of rime accretion by graupel. Atmos. Res. 43, 277–295. https://doi.org/10.1016/S0169-8095(96)00043-9.

Cecil, D.J., Buechler, D.E., Blakeslee, R.J., 2014. Gridded lightning climatology from TRMM-LIS and OTD: Dataset description. Atmos. Res. 135–136, 404–414. https://doi.org/10.1016/j.atmosres.2012.06.028.

Choudhury, B.A., Konwar, M., Hazra, A., Mohan, G.M., Pithani, P., Ghude, S.D., Deshamukhya, A., Barth, M.C., 2020. A diagnostic study of cloud physics and lightning flash rates in a severe pre-monsoon thunderstorm over Northeast India. Q. J. R. Meteorol. Soc. 146, 1901–1922. https://doi.org/10.1002/qj.3773.

Christian, H.J., Blakeslee, R.J., Boccippio, D.J., Boeck, W.L., Buechler, D.E., Driscoll, K. T., Goodman, S.J., Hall, J.M., Koshak, W.J., Mach, D.M., Stewart, M.F., 2003. Global frequency and distribution of lightning as observed from space by the Optical Transient Detector. J. Geophys. Res.-Atmos. 108 https://doi.org/10.1029/2002JD002347. ACL 4-1-ACL 4-15.

Comellas Prat, A., Federico, S., Torcasio, R.C., Fierro, A.O., Dietrich, S., 2021. Lightning data assimilation in the WRF-ARW model for short-term rainfall forecasts of three severe storm cases in Italy. Atmos. Res. 247, 105246 https://doi.org/10.1016/j.atmosres.2020.105246.

Das, S., Sarkar, A., Mohanty, U.C., Tyagi, A., Sikka, D.R., Joseph, P.V., Rathore, L.S., Habib, A., Baidya, S.K., Sonam, K., 2014. The SAARC STORM: a coordinated field experiment on severe thunderstorm observations and regional modeling over the South Asian Region. Bull. Am. Meteorol. Soc. 95, 603–617. https://doi.org/10.1175/BAMS-D-12-00237.1.

Das, S., Sarkar, A., Das, M.K., Rahman, M.M., Islam, M.N., 2015. Composite characteristics of Nor'westers based on observations and simulations. Atmos. Res. 158–159, 158–178. https://doi.org/10.1016/j.atmosres.2015.02.009.

Deierling, W., Petersen, W.A., 2008. Total lightning activity as an indicator of updraft characteristics. J. Geophys. Res.-Atmos. 113 https://doi.org/10.1029/2007JD009598.

Dementyeva, S.O., Ilin, N.V., Mareev, E.A., 2015. Calculation of the lightning potential index and electric field in numerical weather prediction models. Izvestiya, Atmosp. Oceanic Phys. 51, 186–192. https://doi.org/10.1134/S0001433815010028.

Dewan, A., Hossain, M.F., Rahman, M.M., Yamane, Y., Holle, R.L., 2017. Recent lightning-related fatalities and injuries in Bangladesh. Weather, Clim. Soc. 9, 575–589. https://doi.org/10.1175/WCAS-D-16-0128.1.

Dwyer, J.R., 2003. A fundamental limit on electric fields in air. Geophys. Res. Lett. 30 https://doi.org/10.1029/2003GL017781.

Fierro, A.O., Reisner, J.M., 2011. High-resolution simulation of the electrification and lightning of Hurricane Rita during the period of rapid intensification. J. Atmos. Sci. 68, 477–494. https://doi.org/10.1175/2010JAS3659.1.

Fierro, A.O., Mansell, E.R., Ziegler, C.L., MacGorman, D.R., 2012. Application of a lightning data assimilation technique in the WRF-ARW model at cloud-resolving scales for the tornado outbreak of 24 May 2011. Mon. Weather Rev. 140, 2609–2627. https://doi.org/10.1175/MWR-D-11-00299.1.

Fierro, A.O., Mansell, E.R., MacGorman, D.R., Ziegler, C.L., 2013. The implementation of an explicit charging and discharge lightning scheme within the WRF-ARW model: benchmark simulations of a continental squall line, a tropical cyclone, and a winter storm. Mon. Weather Rev. 141, 2390–2415. https://doi.org/10.1175/MWR-D-12-00278.1.

Fierro, A.O., Clark, A.J., Mansell, E.R., MacGorman, D.R., Dembek, S.R., Ziegler, C.L., 2015. Impact of storm-scale lightning data assimilation on WRF-ARW precipitation

forecasts during the 2013 warm season over the contiguous United States. Mon. Weather Rev. 143, 757–777. https://doi.org/10.1175/MWR-D-14-00183.1.
Fiori, E., Lagasio, M., Parodi, A., Procopio, R., Smorgonskiy, A., Rachidi, F., Diendorfer, G., 2016. Implementation and performance analysis of the lightning potential index as a forecasting tool. In: 2016 33rd International Conference on Lightning Protection (ICLP), pp. 1–6. https://doi.org/10.1109/ICLP.2016.7791514.
Galway, J.G., 1956. The lifted index as a predictor of latent instability. Bull. Am. Meteorol. Soc. 37, 528–529. https://doi.org/10.1175/1520-0477-37.10.528.
Gardiner, B., Lamb, D., Pitter, R., Hallett, J., 1985. Measurements of initial electric field and ice particle charges in Montana summer thunderstorms. J. Geophys. Res. 90, 6079–6086.
Gaskell, W., 1981. A laboratory study of the inductive theory of thunderstorm electrification. Q. J. R. Meteorol. Soc. 107, 955–966. https://doi.org/10.1002/qj.49710745413.
George, J., 1960. Weather Forecasting for Aeronautics, 41. Academic Press, New York.
Gharaylou, M., Farahani, M.M., Hosseini, M., Mahmoudian, A., 2019. Numerical study of performance of two lightning prediction methods based on: lightning potential index (LPI) and electric POTential difference (POT) over Tehran area. J. Atmos. Sol. Terr. Phys. 193, 105067 https://doi.org/10.1016/j.jastp.2019.105067.
Goines, D.C., Kennedy, A.D., 2018. Precipitation from a multiyear database of convection-allowing WRF simulations. J. Geophys. Res.-Atmos. 123, 2424–2453. https://doi.org/10.1002/2016JD026068.
Goyal, S., Kumar, A., Sangar, G., Mohapatra, M., 2016. Severe thunderstorm activity over Bihar on 21st April, 2015: a simulation study by satellite based nowcasting technique. In: Proc.SPIE. https://doi.org/10.1117/12.2222740.
Grell, G.A., 1993. Prognostic evaluation of assumptions used by cumulus parameterizations. Mon. Weather Rev. 121, 764–787. https://doi.org/10.1175/1520-0493(1993)121%3C0764:PEOAUB%3E2.0.CO;2.
Gurevich, A.V., Milikh, G.M., Roussel-Dupre, R., 1992. Runaway electron mechanism of air breakdown and preconditioning during a thunderstorm. Phys. Lett. A 165, 463–468. https://doi.org/10.1016/0375-9601(92)90348-P.
Holle, R.L., 2008. Annual rates of lightning fatalities by country. In: 20th International Lightning Detection Conference.
Hong, S.-Y., Noh, Y., Dudhia, J., 2006. A new vertical diffusion package with an explicit treatment of entrainment processes. Mon. Weather Rev. 134, 2318–2341. https://doi.org/10.1175/MWR3199.1.
Huffman, G.J., Stocker, E.F., Bolvin, D.T., Nelkin, E.J., Tan, J., 2019. In: Savtchenko, Andrey, Greenbelt, M.D. (Eds.), GPM IMERG Final Precipitation L3 1 day 0.1 degree x 0.1 degree V06. Goddard Earth Sciences Data and Information Services Center (GES DISC). aaaa. https://doi.org/10.5067/GPM/IMERGDF/DAY/06.
Jayaratne, E.R., Saunders, C.P.R., Hallett, J., 1983. Laboratory studies of the charging of soft-hail during ice crystal interactions. Q. J. R. Meteorol. Soc. 109, 609–630. https://doi.org/10.1002/qj.49710946111.
Karmakar, S., Alam, M., 2017. Use of Radar and Satellite imageries in the study of Nor'westers in Bangladesh. J. NOAMI. 34, 17–32.
Karmakar, S., Quadir, D., Das, M., 2017. Numerical simulation of physical and dynamical characteristics associated with the severe thunderstorm on April 5, 2015 at Kushtia and Jhenaidah. Nat. Hazards 86, 1127–1146. https://doi.org/10.1007/s11069-016-2733-y.
Lagasio, M., Parodi, A., Procopio, R., Rachidi, F., Fiori, E., 2017. Lightning potential Index performances in multimicrophysical cloud-resolving simulations of a back-building mesoscale convective system: the Genoa 2014 event. J. Geophys. Res.-Atmos. 122, 4238–4257. https://doi.org/10.1002/2016JD026115.
Lang, T.J., Rutledge, S.A., Wiens, K.C., 2004. Origins of positive cloud-to-ground lightning flashes in the stratiform region of a mesoscale convective system. Geophys. Res. Lett. 31 https://doi.org/10.1029/2004GL019823.
Litta, A.J., Mohanty, U.C., 2008. Simulation of a severe thunderstorm event during the field experiment of STORM programme 2006, using WRF—NMM model. Curr. Sci. 00113891, 95.
Lutgens, F.K., Tarbuck, E.J., Tasa, D.G., 2013. The Atmosphere: An Introduction to Meteorology, 12, th. ed. Pearson Education Inc., Illinois.
Lynn, B., Yair, Y., 2010. Prediction of lightning flash density with the WRF model. Adv. Geosci. 23, 11–16. https://doi.org/10.5194/adgeo-23-11-2010.
Lynn, B.H., Yair, Y., Price, C., Kelman, G., Clark, A.J., 2012. Predicting cloud-to-ground and intracloud lightning in weather forecast models. Weather Forecast. 27, 1470–1488. https://doi.org/10.1175/WAF-D-11-00144.1.
MacGorman, D.R., Straka, J.M., Ziegler, C.L., 2001. A Lightning Parameterization for Numerical Cloud Models. J. Appl. Meteorol. 40, 459–478. https://doi.org/10.1175/1520-0450(2001)040<0459:ALPFNC>2.0.CO;2.
Mansell, E.R., MacGorman, D.R., Ziegler, C.L., Straka, J.M., 2005. Charge structure and lightning sensitivity in a simulated multicell thunderstorm. J. Geophys. Res.-Atmos. 110 https://doi.org/10.1029/2004JD005287.
Mansell, E.R., Ziegler, C.L., Bruning, E.C., 2010. Simulated electrification of a small thunderstorm with two-moment bulk microphysics. J. Atmos. Sci. 67, 171–194. https://doi.org/10.1175/2009JAS2965.1.
Markowski, P., Richardson, Y., 2011. Mesoscale Meteorology in Midlatitudes. John Wiley & Sons.
Mason, I.B., 2003. Binary events. Forecast Verification 37–76.
McCaul Jr., E.W., Goodman, S.J., LaCasse, K.M., Cecil, D.J., 2009. Forecasting lightning threat using cloud-resolving model simulations. Weather Forecast. 24, 709–729. https://doi.org/10.1175/2008WAF2222152.1.
Miller, K., Gadian, A., Saunders, C., Latham, J., Christian, H., 2001. Modelling and observations of thundercloud electrification and lightning. Atmos. Res. 58, 89–115. https://doi.org/10.1016/S0169-8095(01)00089-8.
Mohan, G.M., Gayatri Vani, K., Hazra, A., Mallick, C., Chaudhari, H.S., Pokhrel, S., Pawar, S.D., Konwar, M., Saha, S.K., Das, S.K., Deshpande, S., Ghude, S., Barth, M.C., Rao, S.A., Nanjundiah, R.S., Rajeevan, M., 2021. Evaluating different lightning parameterization schemes to simulate lightning flash counts over Maharashtra, India. Atmos. Res. 255, 105532 https://doi.org/10.1016/j.atmosres.2021.105532.
NCEP, 2000. NCEP FNL Operational Model Global Tropospheric Analyses, Continuing from July 1999. https://doi.org/10.5065/D6M043C6.
Price, C., Rind, D., 1992. A simple lightning parameterization for calculating global lightning distributions. J. Geophys. Res.-Atmos. 97, 9919–9933. https://doi.org/10.1029/92JD00719.
Rabbani, K.M.G., Das, S., Panda, S.K., Kabir, A., Mallik, M.A.K., 2021. Physical and dynamical characteristics of thunderstorms over Bangladesh based on radar, satellite, upper-air observations, and WRF model simulations. Pure Appl. Geophys. 178, 3747–3767. https://doi.org/10.1007/s00024-021-02847-3.
Reynolds, S.E., Brook, M., Gourley, M.F., 1957. Thunderstorm charge separation. J. Atmos. Sci. 14, 426–436. https://doi.org/10.1175/1520-0469(1957)014<0426:TCS>2.0.CO;2.
Roberts, N.M., Lean, H.W., 2008. Scale-selective verification of rainfall accumulations from high-resolution forecasts of convective events. Mon. Weather Rev. 136, 78–97. https://doi.org/10.1175/2007MWR2123.1.
Roebber, P.J., 2009. Visualizing multiple measures of forecast quality. Weather Forecast. 24, 601–608. https://doi.org/10.1175/2008WAF2222159.1.
Saunders, C.P.R., Peck, S.L., 1998. Laboratory studies of the influence of the rime accretion rate on charge transfer during crystal/graupel collisions. J. Geophys. Res.-Atmos. 103, 13949–13956. https://doi.org/10.1029/97JD02644.
Saunders, C.P.R., Keith, W.D., Mitzeva, R.P., 1991. The effect of liquid water on thunderstorm charging. J. Geophys. Res.-Atmos. 96, 11007–11017. https://doi.org/10.1029/91JD00970.
Skamarock, W.C., Klemp, J.B., Dudhia, J., Gill, D.O., Liu, Z., Berner, J., Wang, W., Powers, J.G., Duda, M.G., Barker, D.M., 2019. A description of the advanced research WRF model version 4. In: National Center for Atmospheric Research: Boulder, CO, USA, 145. https://doi.org/10.5065/1DFH-6P97.
Skok, G., Roberts, N., 2016. Analysis of Fractions Skill score properties for random precipitation fields and ECMWF forecasts. Q. J. R. Meteorol. Soc. 142, 2599–2610. https://doi.org/10.1002/qj.2849.
Sturtevant, J.S., 1995. The Severe Local Storm Forecasting Primer, 1st. Weather Scratch Meteorological Services.
Takahashi, T., 1978. Riming Electrification as a charge Generation Mechanism in Thunderstorms. J. Atmos. Sci. 35, 1536–1548. https://doi.org/10.1175/1520-0469(1978)035<1536:REAACG>2.0.CO;2.
Takahashi, T., 1984. Thunderstorm Electrification—a Numerical Study. J. Atmos. Sci. 41, 2541–2558. https://doi.org/10.1175/1520-0469(1984)041<2541:TENS>2.0.CO;2.
Tessendorf, S.A., Miller, L.J., Wiens, K.C., Rutledge, S.A., 2005. The 29 June 2000 supercell observed during STEPS. Part I: kinematics and microphysics. J. Atmos. Sci. 62, 4127–4150. https://doi.org/10.1175/JAS3585.1.
Torcasio, R.C., Federico, S., Comellas Prat, A., Panegrossi, G., Adderio, L.P., Dietrich, S., 2021. Impact of lightning data assimilation on the short-term precipitation forecast over the Central Mediterranean Sea. Remote Sens. https://doi.org/10.3390/rs13040682.
Umakanth, N., Satyanarayana, G.Ch., Simon, B., Rao, M.C., Babu, N.R., 2020. Analysis of lightning flashes over Bangladesh. In: AIP Conference Proceedings, 2220, p. 140041. https://doi.org/10.1063/5.0001294.
Williams, E.R., Geotis, S.G., Renno, N., Rutledge, S.A., Rasmussen, E., Rickenbach, T., 1992. A radar and electrical study of tropical "hot towers.". J. Atmos. Sci. 49, 1386–1395. https://doi.org/10.1175/1520-0469(1992)049<1386:ARAESO>2.0.CO;2.
Wong, J., Barth, M.C., Noone, D., 2013. Evaluating a lightning parameterization based on cloud-top height for mesoscale numerical model simulations. Geosci. Model Dev. 6, 429–443. https://doi.org/10.5194/gmd-6-429-2013.
Yair, Y., 2018. Lightning hazards to human societies in a changing climate. Environ. Res. Lett. 13, 123002.
Yair, Y., Lynn, B., Price, C., Kotroni, V., Lagouvardos, K., Morin, E., Mugnai, A., del Llasat, M.C., 2010. Predicting the potential for lightning activity in Mediterranean storms based on the Weather Research and forecasting (WRF) model dynamic and microphysical fields. J. Geophys. Res.-Atmos. 115 https://doi.org/10.1029/2008JD010868.
Yamane, Hayashi, T., Kiguchi, M., Akter, F., Dewan, A., 2013. Synoptic Situations of Severe Local Convective Storms during the Pre-Monsoon season in Bangladesh. Int. J. Climatol. 33, 725–734. https://doi.org/10.1002/joc.3460.
Zepka, G.S., Pinto Jr., O., Saraiva, A.C.V., 2014. Lightning forecasting in southeastern Brazil using the WRF model. Atmos. Res. 135, 344–362. https://doi.org/10.1016/j.atmosres.2013.01.008.
Ziegler, C.L., MacGorman, D.R., 1994. Observed lightning morphology relative to modeled space charge and electric field distributions in a tornadic storm. J. Atmos. Sci. 51, 833–851. https://doi.org/10.1175/1520-0469(1994)051<0833:OLMRTM>2.0.CO;2.
Ziegler, C.L., MacGorman, D.R., Dye, J.E., Ray, P.S., 1991. A model evaluation of noninductive graupel-ice charging in the early electrification of a mountain thunderstorm. J. Geophys. Res.-Atmos. 96, 12833–12855. https://doi.org/10.1029/91JD01246.